Topological band engineering and tunable thermal Hall effect in trimerized Lieb lattice ferromagnets

Fengjun Zhuo, Jian Kang, Zhenxiang Cheng, Aurélien Manchon

Topological band engineering and tunable thermal Hall effect in trimerized Lieb lattice ferromagnets

Fengjun Zhuo (卓冯骏),[1,2,*] Jian Kang,[1] Zhenxiang Cheng,[3] and Aurélien Manchon[4,†]

[1]*School of Physical Science and Technology, ShanghaiTech University, Shanghai 201210, China*
[2]*King Abdullah University of Science and Technology (KAUST), Physical Science and Engineering Division (PSE), Thuwal 23955-6900, Saudi Arabia*
[3]*Institute for Superconducting and Electronic Materials, Australian Institute of Innovative Materials, University of Wollongong, Innovation Campus, Squires Way, North Wollongong, NSW 2500, Australia*
[4]*Aix Marseille Univ, CNRS, CINAM, Marseille 13288, France*

We theoretically study the topological properties of magnons and the relevant magnon thermal Hall effect in trimerized Lieb lattice ferromagnets in the presence of next-nearest-neighbor Dzyaloshinskii-Moriya interactions. By calculating the magnon band structures and their Chern numbers with the linear spin-wave theory, we show that the system can undergo a phase transition between a magnonic topological insulator phase and a magnonic trivial insulator phase. The main results are presented in the form of topological phase diagrams, where the Chern numbers or magnon thermal Hall conductivity is shown as a function of the two lattice trimerization parameters. We find a sharp change of the thermal Hall conductivity across the critical point of phase transformations associated with topological nontrivial edge states. The behaviors reflect that the existence of trimerizations breaks the $\mathbf{C}_4$ rotational symmetry of the Lieb lattice. Finally, we show that our theoretical predictions could be experimentally realized in high-temperature cuprate superconductors or organic magnetic materials.

I. INTRODUCTION

Over the past decade, the topological band theory has empowered us to discover new classes of topological materials and understand salient characteristics of topological states in condensed matter physics [1–6]. It is also used to explore new kinds of exotic particles, e.g., Majorana fermions [7, 8], axions [9, 10], spinons [11, 12], magnetic monopoles [13–15], fractionally charged vortices [16], etc., which could potentially be exploited in high-performance electronics, spintronics and topological quantum computation [17–20].

On the other hand, the band topology has been extensively studied in systems consisting of bosonic collective excitations, e.g., photons [21–23], phonons [24, 25], magnetic solitons [26, 27] and magnons [28–31]. A few recent works have reported that magnons can propagate over a long distance without missing spin information in magnetic insulators exhibiting both low energy consumption and long coherence length, which bears a great potential to realize next-generation low-dissipation memory devices [32–34]. Different from electrons, magnons are charge-neutral quasiparticles immune to the Lorentz force due to the external electric field. Meanwhile, the topology of magnons cannot be investigated via the standard Hall effect under a magnetic field-driven Lorentz force. But a transverse thermal current and thermal Hall conductivity are induced by the magnon edge current in the presence of a thermal gradient—the so-called magnon thermal Hall effect (THE) [35]. The finite thermal Hall conductivity could be attributed to an antisymmetric interaction such as Dzyaloshinskii-Moriya interaction (DMI) [36, 37], which induces nonzero Berry curvatures acting as an effective Lorentz force [38–41]. More recently, intensive research of topological magnonics has been performed on various complex lattices, e.g., pyrochlore [42, 43], triangular [44], honeycomb [45–47], kagome [48–51], and Lieb lattices [52–54].

The two-dimensional Lieb lattice, or the line-centered square lattice as shown in Fig. 1(a), was first proposed by Lieb in 1989 when discovering the ferromagnetism on such a lattice due to the flat bands by the Hubbard model of the itinerant-electron [55]. Subsequently, various interesting physical properties of the Lieb lattice have been proposed, e.g., ground-state ferromagnetism [56, 57], topological states [58, 59], superconductivity and superfluidity [60–62]. However, most previous works focus on the theoretical models, since the experimental realization of the Lieb lattice in condensed matter physics has not yet been achieved. Recently, the Lieb lattice has been realized in several artificial systems, such as photonics [63, 64], ultracold atoms in optical lattices [65, 66], and surface patterning techniques [67, 68].

In this paper, we study the magnon band topology and the magnon thermal Hall effect in a trimerized Lieb lattice ferromagnet with the next-nearest-neighbor (NNN) DMI as illustrated in Fig. 1(a). The unit cell in the green dashed diamond is formed by three spin sublattices A, B, and C represented by red, blue and green circles, respectively. We show the topological phase diagrams characterized by the Chern numbers and magnon thermal Hall conductivity on the trimerization parameter plane. We find a topological phase transition between a magnonic topological insulator (mTI) and a magnonic trivial insulator. The phase transition is accompanied by the change of nontrivial edge states and can be experimentally detected by the sharp change of the thermal Hall conductivity. Finally, the candidate materials for an experimental realization are discussed.

The rest of this paper is organized as follows. In Sec. II we present details of our theoretical model and derive the

* zhuofj@shanghaitech.edu.cn
† aurelien.manchon@univ-amu.fr

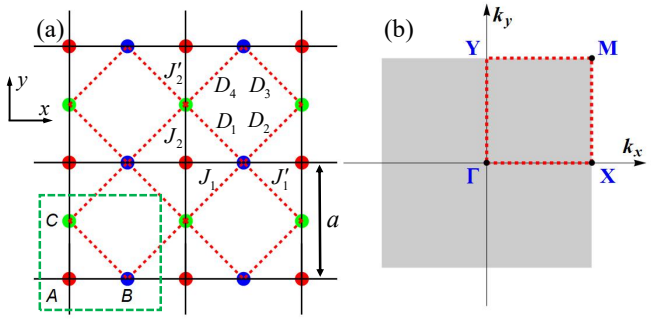

Figure 1. (a) Schematics for the trimerized Lieb lattice ferromagnet. The black solid lines and the red dashed line represent the nearest-neighboring ferromagnetic exchange interactions and next-nearest-neighbor DMI, respectively. The unit cell is shown as a dotted green square. a represents the lattice constant. (b) The first Brillouin zone of the reciprocal lattice.

magnonic tight-binding Hamiltonian. Detailed numerical results are presented in Sec. III, including the topological phase diagram, magnon band structures, magnonic edge states, thermal Hall conductivity, and material consideration. Finally, we end the paper with a Conclusion in Sec. IV.

II. MODEL AND METHODS

We consider a collinear ferromagnet with localized spins on a two-dimensional Lieb lattice as schematically shown in Fig. 1(a), whose spin Hamiltonian is given by

$$\begin{aligned}\mathcal{H} = &-\sum_{\langle ij\rangle} J_{ij}\boldsymbol{S}_i\cdot\boldsymbol{S}_j - K\sum_i S_{iz}^2 \\ &+\sum_{\langle ij\rangle} D_{ij}\epsilon_{ij}\hat{z}\cdot(\boldsymbol{S}_i\times\boldsymbol{S}_j)\,,\end{aligned} \tag{1}$$

where $\boldsymbol{S}_i$ is the vector of spin operators at site i. The first term describes nearest-neighboring (NN) ferromagnetic exchange interactions ($J_{ij}>0$) between sites AB and AC. The second term represents an easy-axis anisotropy ($K>0$) with the z-axis identified as the easy axis. The last term is the out-of-plane NNN DMI between sites BC, where D_{ij} is the DMI strength. ϵ_{ij} corresponds to the magnetic flux, which depends on the lattice geometry and follows the Moriya rules [37] with $+1/-1$ for clockwise/anticlockwise case. Other high-order terms are neglected in this paper, such as the dipole-dipole interaction [69, 70]. A trimerized Lieb lattice is determined by two trimerization parameters δ_1 in A-B bonds along the x direction and δ_2 in A-C bonds along the y direction, which describe the response of the couplings to the displacements of sublattices. Here, we expand the ferromagnetic coupling and DMI following the same methodology in Refs. [71, 72]. Specifically, J_{ij} and D_{ij} are modulated around its equilibrium value J and D with different coefficients as indicated in

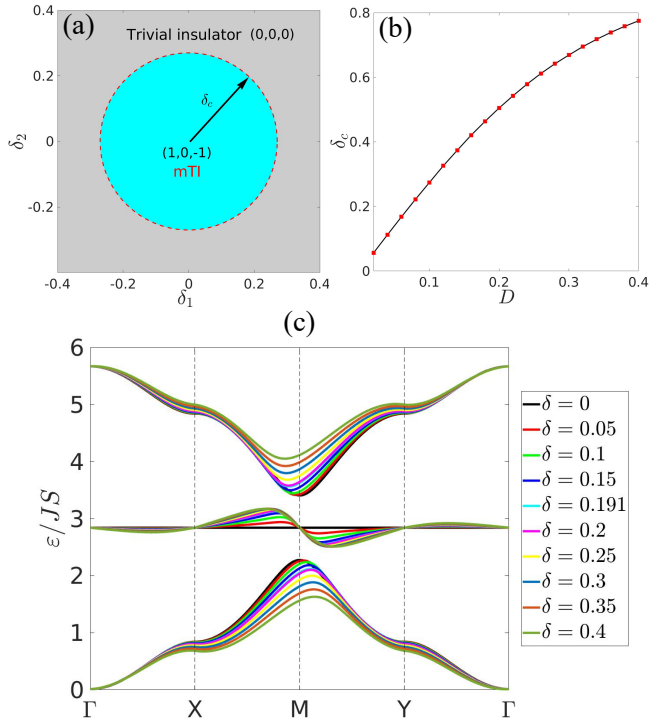

Figure 2. (a) Topological phase diagram of the trimerized Lieb lattice for $D=0.1$. Each topological phase is characterized by sets of Chern numbers (C_1, C_2, C_3). (b) The critical value of phase transition δ_c as a function of the DMI strength D. (c) The magnon band structure with different trimerization $\delta_1=\delta_2=\delta$ when $D=0.1$. $\delta=0.191$ is the critical value of phase transition.

Fig. 1(a),

$$\begin{aligned} J_i &= (1+\delta_i)\,J, \\ J_i' &= (1-\delta_i)\,J, \\ D_1 &= \sqrt{(1+\delta_1)^2+(1+\delta_2)^2}D, \\ D_2 &= \sqrt{(1-\delta_1)^2+(1+\delta_2)^2}D, \\ D_3 &= \sqrt{(1-\delta_1)^2+(1-\delta_2)^2}D, \\ D_4 &= \sqrt{(1+\delta_1)^2+(1-\delta_2)^2}D. \end{aligned} \tag{2}$$

J_1 (J_2) indicates intracell NN ferromagnetic exchange interaction between sublattice A and sublattice B (C) inside a unit cell, as shown in Fig. 1(a). J_1' (J_2') indicates intercell NN ferromagnetic exchange interaction between sublattice A and sublattice B (C) between two NN unit cells. However, the ideal Lieb lattice has been studied by setting both δ_1 and δ_2 equal to zero. In this case, isotropic NN ferromagnetic exchange interactions and NNN DMI are given by $J_{ij}=J$ and $D_{ij}=D$, respectively. Note that the simultaneous changes of ferromagnetic interaction and DMI will preserve the collinear ferromagnetic ground state, since the DMI is well below the threshold value for a phase transition of magnetic configuration.

We now turn to a linear spin-wave theory to obtain the tight-binding magnon Hamiltonian in the momentum space. Using the Holstein-Primakoff transformations [73], we ex-

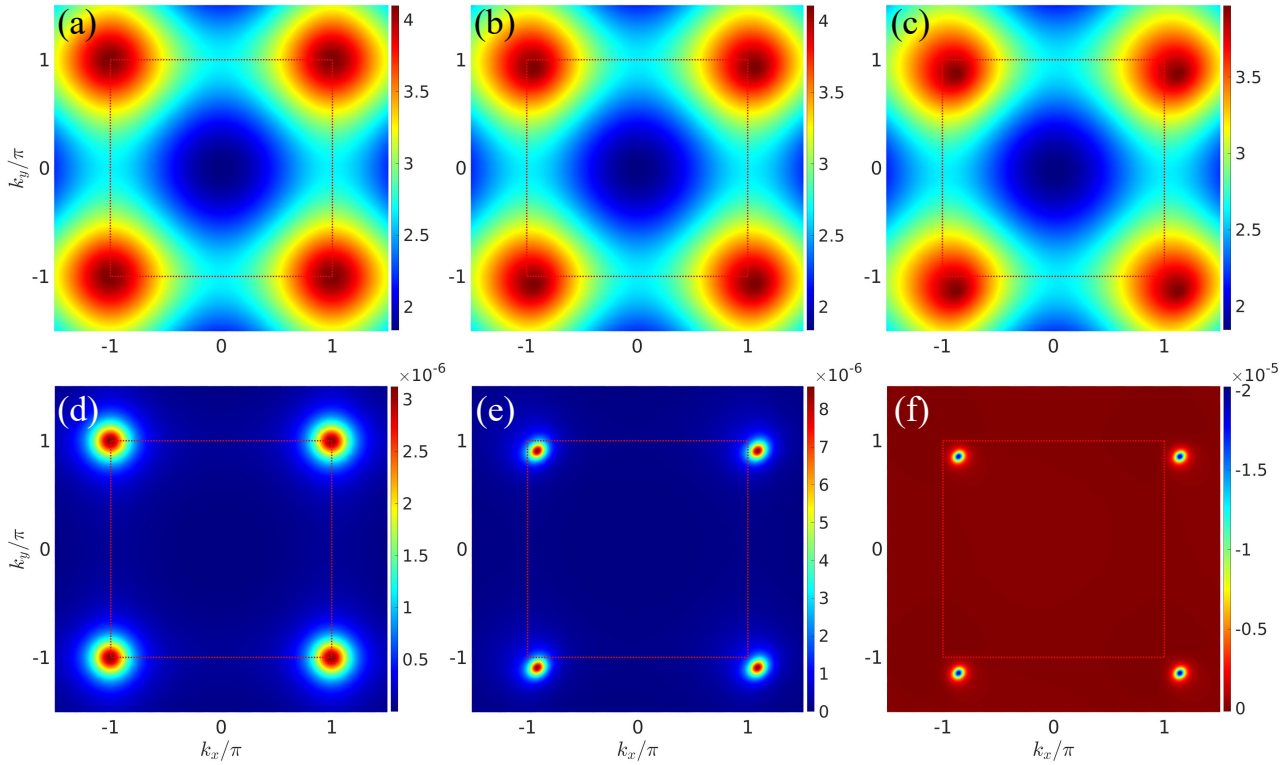

Figure 3. (a-c) The dispersions of the lower magnon band for $\delta_1 = \delta_2 = \delta = 0$, 0.1 and 0.25, respectively. (d-f) Corresponding Berry curvatures of the lower magnon band. The dotted red lines denote the edges of the first Brillouin zone.

press the spin operators in Eq. (1) in terms of magnon creation operator $\hat{b}_i^\dagger$ and annihilation operator $\hat{b}_i$: $S_i^+ = \sqrt{2S - b^\dagger b} b_i$, $S_i^+ = b_i^\dagger \sqrt{2S - b^\dagger b_i}$ and $S_i^z = S - b_i^\dagger b_i$, where we introduce the magnon ladder operators $S_i^\pm = S_i^x \pm i S_i^y$. In the low temperature limit, the square roots can be expanded in powers of $1/\sqrt{S}$ when considering $2S \gg \langle n_i \rangle = \left\langle b_i^\dagger b_i \right\rangle$. After a Fourier transformation, Eq. (1) becomes $\mathcal{H} = -S \sum_{\boldsymbol{k}} \Psi_{\boldsymbol{k}}^\dagger H(\boldsymbol{k}) \Psi_{\boldsymbol{k}}$, where the magnonic tight-binding Hamiltonian H is a 3×3 matrix in the basis $\Psi_{\boldsymbol{k}}^\dagger = \left(b_A^\dagger, b_B^\dagger, b_C^\dagger\right)$ given by

$$H = \begin{pmatrix} -m_0 & \gamma_1 & \gamma_2 \\ \gamma_1^* & -m_0 & i\mu \\ \gamma_2^* & -i\mu^* & -m_0 \end{pmatrix}, \tag{3}$$

where $m_0 = 4J + \sum_{n=1}^4 D_n + 2K$, $\gamma_i = J_i e^{-i\boldsymbol{k}\cdot\boldsymbol{\alpha}_i} + J_i' e^{i\boldsymbol{k}\cdot\boldsymbol{\alpha}_i}$, and $\mu = -D_1 e^{-i\boldsymbol{k}\cdot\boldsymbol{\beta}_2} - D_3 e^{i\boldsymbol{k}\cdot\boldsymbol{\beta}_2} + D_2 e^{-i\boldsymbol{k}\cdot\boldsymbol{\beta}_1} + D_4 e^{i\boldsymbol{k}\cdot\boldsymbol{\beta}_1}$. Here $\boldsymbol{\alpha}_1 = (1/2, 0)\, a$, $\boldsymbol{\alpha}_2 = (0, 1/2)\, a$ and $\boldsymbol{\beta}_1 = (1/2, 1/2)\, a$, $\boldsymbol{\beta}_2 = (-1/2, 1/2)\, a$ are the linking vectors connecting NN and NNN sites, respectively.

In comparison with electronic systems, the absence of Fermi surface in bosonic systems will lead to the ill-defined magnonic Chern number. However, the magnonic Chern number for the nth magnonic bulk band can still be defined as the integration of its Berry curvature $\Omega_{n\boldsymbol{k}}^z$ over the Brillouin zone (BZ) [Fig. 1(b)] in a similar way,

$$C_n = \frac{1}{2\pi} \int_{BZ} dk^2 \Omega_{n\boldsymbol{k}}^z. \tag{4}$$

and the Berry curvature of magnons $\Omega_{n\boldsymbol{k}}^z$ is defined as

$$\Omega_{n\boldsymbol{k}}^z = -2 \sum_{m \neq n} \mathrm{Im} \frac{\langle \psi_{n\boldsymbol{k}} | \partial_{k_x} H | \psi_{m\boldsymbol{k}} \rangle \langle \psi_{m\boldsymbol{k}} | \partial_{k_y} H | \psi_{n\boldsymbol{k}} \rangle}{\left(\varepsilon_{n\boldsymbol{k}} - \varepsilon_{m\boldsymbol{k}}\right)^2}, \tag{5}$$

where $\psi_{n\boldsymbol{k}}$ and $\varepsilon_{n\boldsymbol{k}}$ are the eigenvectors and eigenvalues of $H(\boldsymbol{k})$ for the nth band, respectively. The magnon thermal Hall conductivity is also related to the Berry curvature and can be calculated using the following formula [74]

$$\kappa_{xy} = -\frac{k_B^2 T}{\hbar} \sum_{n=1}^3 \int_{BZ} \frac{d^2k}{(2\pi)^2} c_2 \left[\rho^B(\varepsilon_{n\boldsymbol{k}})\right] \Omega_{n\boldsymbol{k}}^z, \tag{6}$$

where $\rho^B(\varepsilon_{n\boldsymbol{k}}) = \left(e^{\varepsilon_{n\boldsymbol{k}}/k_B T} - 1\right)^{-1}$ is the Bose-Einstein distribution. The weighting function is given by $c_2 = (1+x)\ln^2 \frac{1+x}{x} - \ln^2 x - 2\mathrm{Li}_2(-x)$, with $\mathrm{Li}_2(x)$ being the polylogarithm function.

To calculate the Chern numbers and thermal Hall conductivity of magnons numerically [cf. Eqs. (4) and (6)], we calculate the Berry curvature [cf. Eq. (5)] following the algorithm of Fukui *et al.* [75] with 1000×1000 points over the BZ. In addition, for the sake of simplicity, the tight-binding magnon

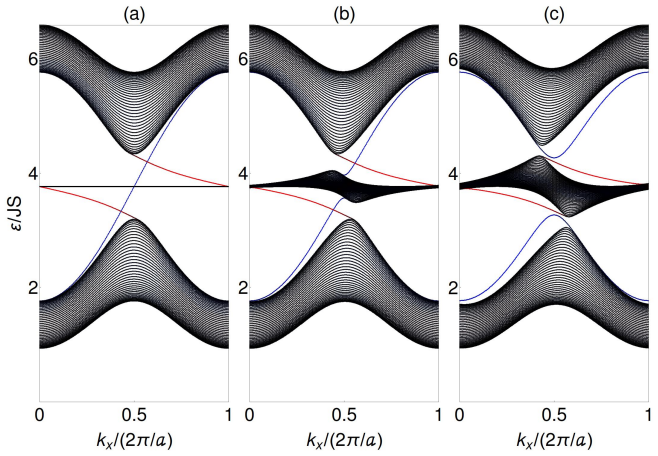

Figure 4. Magnon band structure with coupled magnonic edge states in a quasi-one-dimensional Lieb ribbon with different trimerization $\delta_1 = \delta_2 = \delta$: (a) $\delta = 0$. (b) $\delta = 0.1$. (c) $\delta = 0.25$. The black lines represent the magnon bulk bands. The blue/red lines are the edge states for the upper/lower edges.

Hamiltonian Eq. (3) is normalized to JS. Meanwhile, energy, temperature and thermal Hall conductivity are expressed in the units of JS, k_BT/JS, and $JS\,(k_B/\hbar)$, respectively. In the following numerical calculations, unless otherwise specified, we set $K = 0.05J$, whereas D, δ_1 and δ_2 are tunable parameters.

III. RESULTS AND DISCUSSION

The main proposal in this work is to identify different topological phases by varying the trimerization parameters δ_1 and δ_2. We first show in Fig. 2(a) a topological phase diagram on the $\delta_1 - \delta_2$ plane, where the two phases are characterized by sets of Chern numbers (C_1, C_2, C_3) of the lower, middle and upper magnon bulk bands, as shown in Fig. 2(c). The system turns out to be a mTI with Chern numbers $(1, 0, -1)$ when $\sqrt{\delta_1^2 + \delta_2^2} < \delta_c$ and a trivial magnonic insulator with zero Chern numbers otherwise. The critical value of phase transition δ_c as a function of the DMI strength D is depicted in Fig. 2(b).

We show in Fig. 2(c) the evolution of the magnon band structures with varying δ when $D = 0.1$, where we consider the case that two trimerization parameters are equivalent ($\delta_1 = \delta_2 = \delta$). As the unit cell of the Lieb lattice consists of three sublattices, it gives three magnon bands after diagonalization of the Hamiltonian (3). The magnon bands are plotted along the Γ−X−M−X−Γ line with high-symmetry points in the Brillouin zone shown in Fig. 1(b). A band structure in the ideal Lieb lattice without trimerization $\delta = 0$ has a perfectly flat magnon band in the middle, which isolates the lower and upper magnon bands symmetrically [52]. The lower and upper dispersive magnon bands are almost equally localized on all three sublattices A, B and C, while the flat middle magnon band is a high-degeneracy eigenspace composed of localized states almost fully localized on the sublattices B and C [76, 77]. Two nontrivial band gaps opens between the three dispersive magnon bands due to the existence of DMI acting as an effective spin-orbit coupling [58]. Meanwhile, the lower and upper magnon bands are topologically nontrivial with Chern numbers $C_1 = 1$ and $C_3 = -1$, respectively, and the middle flat band is a topologically trivial band with Chern number $C_2 = 0$. When the trimerization is included ($\delta \neq 0$), the middle magnon band becomes out-of-flatness, meanwhile, the top of the lower band and the bottom of the upper band shift to the right (Y point) and left (X point) with increasing δ, respectively. In addition, there are three different cases: (a) When $0 \leq \delta < 0.191$, the Chern numbers of the bands from bottom to top are $(1, 0, -1)$ and the magnonic system stays in a mTI phase. (b) At a critical value of $\delta = 0.191$, a topological phase transition occurs. (c) When $\delta > 0.191$, the lower and upper magnon bands become topologically trivial with Chern numbers $C_1 = C_3 = 0$, while the system reduces to a trivial magnonic insulator. As the trimerization is increased, the dispersive topologically nontrivial bands are pushed away from the flat band and they flatten out progressively, which corresponds to the decoupling of the sublattices B and C from the neighboring sublattices A outside the unit cell as depicted in Fig. 1(a). Furthermore, we consider the fully-trimerized limit $\delta = 1$ with a small DMI strength ($D \ll J$), where the intracell NN ferromagnetic exchange interactions reach a maximum ($J_1 = J_2 = 2J$) and the intercell interactions are turned off ($J_1' = J_2' = 0$). Since neighboring unit cells almost do not "talk" to each other in this case, the system is reduced to an array of isolated trimers on a square lattice and the magnon bands split into three flat bands separated by two large trivial gaps, that the energy states are strongly localized [78]. Thus a large trimerization degenerates the system into a trivial magnonic insulator from a magnonic topological insulator.

To better understand the underlying physics of the two topological magnonic phases, it is instructive to investigate three representative cases: $\delta = 0$, 0.1, and 0.25. Since the lower band is always more populated for magnons than the upper band at low temperatures, we will focus on the lower band in the following discussion. In figures 3(a)-(c), we plot the lower magnon bands for $\delta = 0$, 0.1, and 0.25, respectively. However, the upper band can be obtained directly by a centrosymmetric reflection about the M point on the middle magnon band as shown in Fig. 2(c). We plot the distribution of Berry curvature $\Omega^z_{n\boldsymbol{k}}$ associated with the lower magnon band for $\delta = 0$, 0.1, and 0.25 in figures 3(d)-(f), respectively. The Berry curvature exhibits higher densities around where the eigenvalue reaches the peaks. We find a universal translation of magnon band [Figures 3(b)-(c)] and Berry curvature [Figures 3(e)-(f)] due to the trimerization. Meanwhile, it is remarkable that the introduction of trimerization breaks the $\mathbf{C}_4$ rotational symmetry of the Lieb lattice. It should be noted that the Berry curvatures are positive in the carmine region (the very bottom of the legend) in Fig. 3(f), which gives a zero Chern number after integrating in the first Brillouin zone.

According to the nonzero Chern numbers, the universal bulk-edge correspondence guarantees that a topological nontrivial band is always accompanied by chiral edge states. To

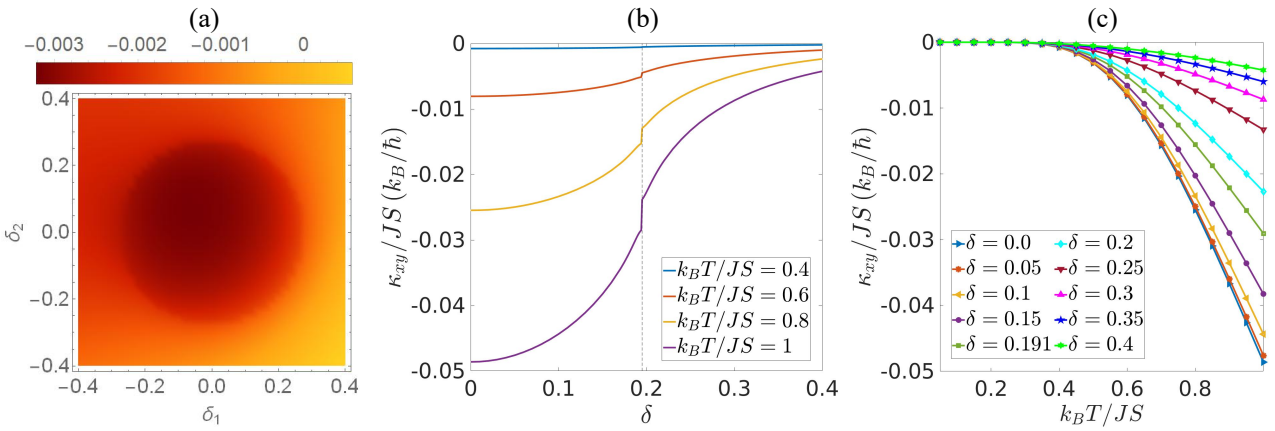

Figure 5. (a) Thermal Hall conductivity κ_{xy} as a function of δ_1 and δ_2 at temperature 0.5 for $D = 0.1$. (b) κ_{xy} as a function of δ at different temperatures. The critical point is shown as a vertical dashed line. (c) Thermal Hall conductivity as a function of temperature for different δ.

better visualize the magnonic edge states, we solved the eigenvalue problem of a quasi-one-dimensional Lieb ribbon with open boundary conditions. In Fig. 4, we present the evolution of the edge-state spectrum. In an ideal Lieb lattice [Fig. 4(a)], the middle bulk band is flat and the edge-state spectrum connect the upper and lower bulk bands. The pair of edge states have uniform slopes $v_g = \partial\varepsilon/\partial k$ (*i.e.*, group velocity) in both band gaps, in other words, they propagate in the same directions: the edge state marked by red lines move from the top left to the bottom right ($v_g < 0$) and the edge state marked by blue lines move from the bottom left to the top right ($v_g > 0$), respectively. Meanwhile, the edge states indicate that the edge magnon currents at upper and down boundaries of the nanoribbon have different motion velocities. The distinct velocities arise due to the propagation directions are determined by the directions of DMI vectors which, in turn, determine the signs of the Berry curvatures. Simultaneously, the magnons must transport energies from the hot side to the cold side adhering to the second law of thermodynamics. In conclusion, our observation confirms that the magnon currents tend to flow predominantly along one of the boundaries, dynamically changing with the direction of the temperature gradient. This behavior vividly reflects the chirality of the magnon edge states [31]. At a small trimerization case ($\delta = 0.1$) in Fig. 4(b), only the bulk bands distort but does not affect the existence of the edge states. Conversely, at a large trimerization case ($\delta = 0.25$) in Fig. 4(c), the edge states are all gapped and trivial, as the Chern numbers of three bulk bands are zero.

Having demonstrated two distinct topological phases for different trimerization parameters, we next turn to discuss the topological properties of magnon THE. In Fig. 5(a), we plot the magnon thermal Hall conductivity κ_{xy} (in unit of $JSk_B/\hbar$) at temperature 0.5 (in unit of k_BT/JS) on the $\delta_1 - \delta_2$ plane, which shows the same phase boundaries as Fig. 2(a). Overall, κ_{xy} decreases with an increasing $\sqrt{\delta_1^2 + \delta_2^2}$. Even though the magnon bands have zero Chern numbers and the edge states become topologically trivial as a trivial magnonic insulator, κ_{xy} does not vanish due to the bosonic statistics (c_2 function in Eq. (6)) that nonuniformly weights the Berry curvature. Furthermore, we plot κ_{xy} as a function of δ at four different temperatures in Fig. 5(b). It shows that κ_{xy} undergoes a sharp decrease across the critical point of phase transformations, which is more striking at higher temperatures due to the enhancement of magnon density. This abrupt change of κ_{xy} is attributed to the vanishing of nontrivial edge states when the system enters a trivial magnonic insulator phase from a mTI phase, as the edge states provide the predominant contribution to the thermal Hall conductivity. In addition, this saltation of the thermal Hall conductivity can also be used to identify the topological phase transition. We also find that this tendency, the decrease of κ_{xy} with increasing δ, is independent of the temperature. Finally, plots of the thermal Hall conductivity κ_{xy} against the temperature for various trimerization parameters δ are depicted in Fig. 5(c). As the temperature increases, κ_{xy} shows a monotonically rising behavior with increasing temperatures. Due to the low magnon current density near absolute zero temperature, the thermal Hall conductivity is expected to be close to zero [74].

Thus far, we have shown a tunable topological magnon excitation in trimerized Lieb lattice ferromagnets. However, the results presented above do not include the magnon-magnon interactions, as we truncate the bosonic Hamiltonian to quadratic order within the linear spin-wave theory as mentioned in Sec. II. Although noninteracting magnons are considered here, it is straightforward to include the magnon-magnon interactions based on our formulation to consider other richer physics [79], since the magnon Hamiltonian can be obtained within the Schwinger-boson representation of spin operators by using self-consistent mean-field theory [80]. Meanwhile the thermal Hall conductivities obtained from both types of representations are approximately identical. Whereas, our results should be valid provided that the temperature is lower than the Curie temperature.

Before concluding, we shall briefly discuss the candidate materials for experimental realizations of our theoretical predictions. In recent years, theoretical studies on the Hubbard models of strongly correlated quantum magnetism in the Lieb lattice have been performed [81–84], which propose that the

most prominent materials are weakly coupled CuO_2 planes in well-known high-temperature cuprate superconductors such as $YBa_2Cu_3O_7$, $La_{2x}Sr_xCuO_4$ or $Bi_2Sr_2CaCu_2O_8$ [85–88]. On the other hand, ferromagnetism in organic materials has been a stirring research field for both fundamental interests and practical applications [89, 90]. Based on density functional theory calculation and tight-binding modeling, it has been reported that the Lieb lattice ferromagnet could be experimentally realized in the framework of covalent-organic compounds [91, 92]. Recently, the realization of two-dimensional magnets in designed structures based on superatomic lattices of zirconium dichloride disks have been demonstrated by using first-principles calculations, including ferromagnetic coloring triangle, antiferromagnetic honeycomb, and ferromagnetic kagome lattices [93]. Meanwhile the NNN DMI may exist on the interface of a layered heterostructure composed of these candidate materials and heavy metals [94]. In addition, since the interactions are susceptible to the distances between atoms, the trimerization on the Lieb lattice could be realized from the lattice distortions induced by applying external mechanical strain or pressure [95–97]. However, more detailed first-principles calculations and experiments are highly desire to investigate the mTI in the future.

IV. CONCLUSION

In conclusion, we have investigated the magnon band topology and thermal Hall effect in the two-dimensional Lieb lattice ferromagnets with DMI. We have theoretically demonstrated that the topological phase of the system can be tuned by two lattice trimerization parameters, while the $\mathbf{C}_4$ rotational symmetry of the Lieb lattice is broken. We also show that the system can undergo a phase transition between a magnonic topological insulator and a magnonic trivial insulator with the change of nontrivial edge states. Furthermore, a sharp change of the thermal Hall conductivity across the phase boundaries was found, which provides a solid signature for experimental detection of the phase transition. In this regard, we hope that our studies could open thrilling perspectives for experimentalists and be applied in future magnonic devices.

ACKNOWLEDGEMENTS

F.Z. was supported by the Double First-Class Initiative Fund of ShanghaiTech University, the Postdoctoral International Exchange Program of China (Grant No. YJ20220302) and King Abdullah University of Science and Technology (KAUST). J.K. acknowledge the support from the National Natural Science Foundation of China (Grant No. 12074276) and the start-up grant of ShanghaiTech University. Z.X.C. thanks Australia Research Council for support (DP190100150). A.M. acknowledges support from the Excellence Initiative of Aix-Marseille Université—A*Midex, a French "Investissements d'Avenir" program.

[1] M. Z. Hasan and C. L. Kane, Rev. Mod. Phys. **82**, 3045 (2010).
[2] M. Z. Hasan and J. E. Moore, Annu. Rev. Condens. Matter Phys. **2**, 55 (2011).
[3] X.-L. Qi and S.-C. Zhang, Rev. Mod. Phys. **83**, 1057 (2011).
[4] B. Yan and S.-C. Zhang, Rep. Prog. Phys. **75**, 096501 (2012).
[5] A. Bansil, H. Lin, and T. Das, Rev. Mod. Phys. **88**, 021004 (2016).
[6] Y. Tokura, K. Yasuda, and A. Tsukazaki, Nat. Rev. Phys. **1**, 126 (2019).
[7] L. Fu and C. L. Kane, Phys. Rev. Lett. **100**, 096407 (2008).
[8] S. Nadj-Perge, I. K. Drozdov, J. Li, H. Chen, S. Jeon, J. Seo, A. H. MacDonald, B. A. Bernevig, and A. Yazdani, Science **346**, 602 (2014).
[9] A. M. Essin, J. E. Moore, and D. Vanderbilt, Phys. Rev. Lett. **102**, 146805 (2009).
[10] D. M. Nenno, C. A. Garcia, J. Gooth, C. Felser, and P. Narang, Nat. Rev. Phys. **2**, 682 (2020).
[11] M. Kohno, O. A. Starykh, and L. Balents, Nat. Phys. **3**, 790 (2007).
[12] S. Yan, D. A. Huse, and S. R. White, Science **332**, 1173 (2011).
[13] C. Castelnovo, R. Moessner, and S. L. Sondhi, Nature **451**, 42 (2008).
[14] X.-L. Qi, T. L. Hughes, and S.-C. Zhang, Phys. Rev. B **78**, 195424 (2008).
[15] X.-L. Qi, R. Li, J. Zang, and S.-C. Zhang, Science **323**, 1184 (2009).
[16] B. Seradjeh, J. E. Moore, and M. Franz, Phys. Rev. Lett. **103**, 066402 (2009).
[17] V. Baltz, A. Manchon, M. Tsoi, T. Moriyama, T. Ono, and Y. Tserkovnyak, Rev. Mod. Phys. **90**, 015005 (2018).
[18] S. Das Sarma, M. Freedman, and C. Nayak, Phys. Rev. Lett. **94**, 166802 (2005).
[19] C. Nayak, S. H. Simon, A. Stern, M. Freedman, and S. Das Sarma, Rev. Mod. Phys. **80**, 1083 (2008).
[20] A. Stern and N. H. Lindner, Science **339**, 1179 (2013).
[21] L. Lu, J. D. Joannopoulos, and M. Soljačić, Nat. Photon. **8**, 821 (2014).
[22] A. B. Khanikaev and G. Shvets, Nat. Photon. **11**, 763 (2017).
[23] T. Ozawa, H. M. Price, A. Amo, N. Goldman, M. Hafezi, L. Lu, M. C. Rechtsman, D. Schuster, J. Simon, O. Zilberberg, *et al.*, Rev. Mod. Phys. **91**, 015006 (2019).
[24] L. Zhang, J. Ren, J.-S. Wang, and B. Li, Phys. Rev. Lett. **105**, 225901 (2010).
[25] R. Süsstrunk and S. D. Huber, Science **349**, 47 (2015).
[26] B. Göbel, I. Mertig, and O. A. Tretiakov, Phys. Rep. **895**, 1 (2021).
[27] Z.-X. Li, Y. Cao, and P. Yan, Phys. Rep. **915**, 1 (2021).
[28] P. A. McClarty, Annu. Rev. Condens. Matter Phys. **13** (2021) .

[29] V. Bonbien, F. Zhuo, A. Salimath, O. Ly, A. Abbout, and A. Manchon, J. Phys. D: Appl. Phys. **55** 103002 (2021).
[30] A. Barman, G. Gubbiotti, S. Ladak, A. O. Adeyeye, M. Krawczyk, J. Gräfe, C. Adelmann, S. Cotofana, A. Naeemi, V. I. Vasyuchka, *et al.*, J. Phys.: Condens. Matter **33**, 413001 (2021).
[31] F. Zhuo, J. Kang, A. Manchon, and Z. Cheng, Adv. Phys. Res. 2300054 (2023).
[32] A. Khitun, M. Bao, and K. L. Wang, J. Phys. D: Appl. Phys. **43**, 264005 (2010).
[33] B. Lenk, H. Ulrichs, F. Garbs, and M. Münzenberg, Phys. Rep. **507**, 107 (2011).
[34] A. V. Chumak, V. I. Vasyuchka, A. A. Serga, and B. Hillebrands, Nat. Phys. **11**, 453 (2015).
[35] H. Katsura, N. Nagaosa, and P. A. Lee, Phys. Rev. Lett. **104**, 066403 (2010).
[36] I. Dzyaloshinsky, J. Phys. Chem. Sol. **4**, 241 (1958).
[37] T. Moriya, Phys. Rev. **120**, 91 (1960).
[38] A. Belabbes, G. Bihlmayer, F. Bechstedt, S. Blügel, and A. Manchon, Phys. Rev. Lett. **117**, 247202 (2016).
[39] A. Manchon, J. Železný, I. M. Miron, T. Jungwirth, J. Sinova, A. Thiaville, K. Garello, and P. Gambardella, Rev. Mod. Phys. **91**, 035004 (2019).
[40] H. Takeda, J. Mai, M. Akazawa, K. Tamura, J. Yan, K. Moovendaran, K. Raju, R. Sankar, K.-Y. Choi, and M. Yamashita, Phys. Rev. Res. **4**, L042035 (2022).
[41] P. Czajka, T. Gao, M. Hirschberger, P. J. Lampen-Kelley, A. Banerjee, N. Quirk, D. G. Mandrus, S. E. Nagler, and N. P. Ong, Nat. Mater. **22**, 36 (2023).
[42] Y. Onose, T. Ideue, H. Katsura, Y. Shiomi, N. Nagaosa, and Y. Tokura, Science **329**, 297 (2010).
[43] A. Mook, J. Henk, and I. Mertig, Phys. Rev. Lett. **117**, 157204 (2016).
[44] K.-S. Kim, K. H. Lee, S. B. Chung, and J.-G. Park, Phys. Rev. B **100**, 064412 (2019).
[45] S. S. Pershoguba, S. Banerjee, J. C. Lashley, J. Park, H. Ågren, G. Aeppli, and A. V. Balatsky, Phys. Rev. X **8**, 011010 (2018).
[46] L. Chen, J.-H. Chung, B. Gao, T. Chen, M. B. Stone, A. I. Kolesnikov, Q. Huang, and P. Dai, Phys. Rev. X **8**, 041028 (2018).
[47] L. Chen, J.-H. Chung, M. B. Stone, A. I. Kolesnikov, B. Winn, V. O. Garlea, D. L. Abernathy, B. Gao, M. Augustin, E. J. G. Santos, and P. Dai, Phys. Rev. X **11**, 031047 (2021).
[48] M. Hirschberger, R. Chisnell, Y. S. Lee, and N. P. Ong, Phys. Rev. Lett. **115**, 106603 (2015).
[49] R. Chisnell, J. S. Helton, D. E. Freedman, D. K. Singh, R. I. Bewley, D. G. Nocera, and Y. S. Lee, Phys. Rev. Lett. **115**, 147201 (2015).
[50] F. Zhuo, H. Li, and A. Manchon, Phys. Rev. B **104**, 144422 (2021).
[51] F. Zhuo, H. Li, and A. Manchon, New J. Phys. **24**, 023033 (2022).
[52] X. Cao, K. Chen, and D. He, J. Phys.: Condens. Matter **27**, 166003 (2015).
[53] M. Yarmohammadi, J. Magn. Magn. Mater. **417**, 208 (2016).
[54] A. Pires, J. Magn. Magn. Mater. **547**, 168941 (2022).
[55] E. H. Lieb, Phys. Rev. Lett. **62**, 1201 (1989).
[56] H. Tasaki, Phys. Rev. Lett. **69**, 1608 (1992).
[57] H. Tasaki, Eur. Phys. J. B **64**, 365 (2008).
[58] A. Zhao and S.-Q. Shen, Phys. Rev. B **85**, 085209 (2012).
[59] W. Beugeling, J. C. Everts, and C. Morais Smith, Phys. Rev. B **86**, 195129 (2012).
[60] S. Miyahara, S. Kusuta, and N. Furukawa, Physica C **460**, 1145 (2007).
[61] A. Julku, S. Peotta, T. I. Vanhala, D.-H. Kim, and P. Törmä, Phys. Rev. Lett. **117**, 045303 (2016).
[62] M. Tylutki and P. Törmä, Phys. Rev. B **98**, 094513 (2018).
[63] R. A. Vicencio, C. Cantillano, L. Morales-Inostroza, B. Real, C. Mejía-Cortés, S. Weimann, A. Szameit, and M. I. Molina, Phys. Rev. Lett. **114**, 245503 (2015).
[64] S. Mukherjee, A. Spracklen, D. Choudhury, N. Goldman, P. Öhberg, E. Andersson, and R. R. Thomson, Phys. Rev. Lett. **114**, 245504 (2015).
[65] S. Taie, H. Ozawa, T. Ichinose, T. Nishio, S. Nakajima, and Y. Takahashi, Sci. Adv. **1**, e1500854 (2015).
[66] F. Schäfer, T. Fukuhara, S. Sugawa, Y. Takasu, and Y. Takahashi, Nat. Rev. Phys. **2**, 411 (2020).
[67] M. R. Slot, T. S. Gardenier, P. H. Jacobse, G. C. van Miert, S. N. Kempkes, S. J. Zevenhuizen, C. M. Smith, D. Vanmaekelbergh, and I. Swart, Nat. Phys. **13**, 672 (2017).
[68] R. Drost, T. Ojanen, A. Harju, and P. Liljeroth, Nat. Phys. **13**, 668 (2017).
[69] R. Shindou, J.-i. Ohe, R. Matsumoto, S. Murakami, and E. Saitoh, Phys. Rev. B **87**, 174402 (2013).
[70] R. Matsumoto, R. Shindou, and S. Murakami, Phys. Rev. B **89**, 054420 (2014).
[71] M. Vozmediano, M. Katsnelson, and F. Guinea, Phys. Rep. **496**, 109 (2010).
[72] Y. Ferreiros and M. A. H. Vozmediano, Phys. Rev. B **97**, 054404 (2018).
[73] T. Holstein and H. Primakoff, Phys. Rev. **58**, 1098 (1940).
[74] R. Matsumoto and S. Murakami, Phys. Rev. Lett. **106**, 197202 (2011).
[75] T. Fukui, Y. Hatsugai, and H. Suzuki, J. Phys. Soc. Jpn. **74**, 1674 (2005).
[76] J. D. Gouveia, I. A. Maceira, and R. G. Dias, Phys. Rev. B **94**, 195132 (2016).
[77] B. Jaworowski, A. Manolescu, and P. Potasz, Phys. Rev. B **92**, 245119 (2015).
[78] N. Swain and M. Karmakar, Phys. Rev. Research **2**, 023136 (2020).
[79] A. L. Chernyshev and P. A. Maksimov, Phys. Rev. Lett. **117**, 187203 (2016).
[80] H. Lee, J. H. Han, and P. A. Lee, Phys. Rev. B **91**, 125413 (2015).
[81] C. Weeks and M. Franz, Phys. Rev. B **82**, 085310 (2010).
[82] K. Noda, K. Inaba, and M. Yamashita, Phys. Rev. A **90**, 043624 (2014).
[83] J. Faúndez, T. N. Jorge, and L. Craco, Phys. Rev. B **97**, 115149 (2018).
[84] L. Oliveira-Lima, N. C. Costa, J. P. de Lima, R. T. Scalettar, and R. R. d. Santos, Phys. Rev. B **101**, 165109 (2020).
[85] V. J. Emery, Phys. Rev. Lett. **58**, 2794 (1987).
[86] M. Beno, L. Soderholm, D. Capone, D. Hinks, J. Jorgensen, J. Grace, I. K. Schuller, C. Segre, and K. Zhang, Appl. Phys. Lett. **51**, 57 (1987).
[87] R. T. Scalettar, D. J. Scalapino, R. L. Sugar, and S. R. White, Phys. Rev. B **44**, 770 (1991).
[88] S. Massidda, J. Yu, and A. Freeman, Physica C **152**, 251 (1988).
[89] J. S. Miller and A. J. Epstein, Angew. Chem. **33**, 385 (1994).
[90] C. Benelli and D. Gatteschi, Chem. Rev. **102**, 2369 (2002).
[91] W. Jiang, H. Huang, and F. Liu, Nat. Commun. **10**, 2207 (2019).
[92] W. Jiang, S. Zhang, Z. Wang, F. Liu, and T. Low, Nano Lett. **20**, 1959 (2020).
[93] Y. Song, W.-H. Dong, K.-R. Hao, S. Du, and L. Zhang, Nano Res. (2023).

[94] H. Yang, J. Liang, and Q. Cui, Nat. Rev. Phys. **5**, 43 (2023).
[95] F. Guinea, M. Katsnelson, and A. Geim, Nat. Phys. **6**, 30 (2010).
[96] L. Webster and J.-A. Yan, Phys. Rev. B **98**, 144411 (2018).
[97] M. Bahramy, B.-J. Yang, R. Arita, and N. Nagaosa, Nat. Commun. **3**, 1 (2012).